

Properties of the gluon recombination functions

Wei Zhu and Zhenqi Shen

Department of Physics, East China Normal University, Shanghai 200062, P.R. China

Abstract

The gluon recombination functions in the twist-4 QCD evolution equations are studied at the leading logarithmic approximation using both the covariant and non-covariant methods. We justify that the infrared singularities in the twist-4 coefficient functions impede us to simply separate the QCD evolution kernels from the coefficient functions at the equivalent particle approximation. In particular, we point out that the gluon recombination functions in the GLR-MQ evolution equation are unavailable. The methods avoiding the IR divergences are discussed, which can be used in the derivations of the evolution kernels and coefficient functions at the higher twist level.

1 Introduction

The QCD evolution equations in the leading order level predict strong rise of parton densities when the Bjorken variable $x_B = Q^2/2p \cdot q$ decrease toward small values. This behavior violates unitarity. Therefore, various models are proposed to modify the twist-2 evolution kernels (i.e., the parton splitting functions). Gribov, Levin and Ryskin [1] first suggest a non-linear evolution equation, in which the evolution kernels (we call them as the gluon recombination functions) are constructed by the fan diagrams. Later Mueller and Qiu [2] calculate the (real) gluon recombination functions at the double leading logarithmic approximation (*DLLA*) in a covariant perturbation framework. The GLR-MQ equation is broadly regarded as a key link from perturbation region to non-perturbation region. This equation was generalized to include the contributions from more higher order corrections in the Glauber-Mueller formula [3]. Following them, a similar evolution equation (we call it as the recombination equation) is derived in a more broad kinematic region (the leading logarithmic (Q^2) approximation-*LLA*(Q^2)) in Ref.[4]. Different from the GLR-MQ equation, the gluon recombination functions in this equation are calculated and summed in the (old-fashioned) time-ordered perturbation theory (TOPT) [5].

In this paper we present the different results of the gluon recombination functions in the above mentioned two evolution equations. The cross section (or structure functions) of deep inelastic electron-proton scattering in a factorization scheme can be factorized into the convolution of coefficient functions with nonperturbative matrix elements, which are defined as the parton distributions in the twist-2 level. The QCD evolution kernels (for example, splitting and recombination functions) are separated from the coefficient functions either in a covariant perturbation theory or in a parton model using TOPT.

It is well known that these two approaches are completely equivalent. However, we find that the infrared (IR) singularities in the twist-4 Feynman diagrams impede us to safely extract the evolution kernels *before* these singularities are cancelled. This result leads to the fact that the gluon recombination functions in the GLR-MQ evolution equation are unavailable. For illustrating our idea in detail, in Sec. 2 we compare two approaches in the derivations of a splitting function in the twist-2 DGLAP equation [6]. Then we show two different derivations of the twist-4 recombination functions in Sec. 3. In Sec. 4 we analyze the IR singularities in the recombination functions, which arise the questions in the derivations of the gluon recombination functions in the covariant theory. The discussions and conclusions are given in Sec. 5.

2 Twist-2 splitting functions

The splitting functions for partons (quarks or gluon) in the twist-2 evolution equations are schematically defined as Fig. 1a. We emphasize that all initial and final partons in Fig.1 should be on-shell, thus the fraction of the momentum and helicity, which is carried by a parton, can be fixed [6]. The physical gauge is convenient in the calculations of the evolution kernels. In this work we take the physical axial gauge and let the light-like vector n to fix the gauge as $n \cdot A = 0$, A being the gluon field, where

$$n^\mu \equiv \frac{1}{\sqrt{2}}(1, 0_\perp, -1),$$

and

$$\bar{n}^\mu \equiv \frac{1}{\sqrt{2}}(1, 0_\perp, 1). \quad (2.1)$$

Therefore, we have

$$n \cdot n = \bar{n} \cdot \bar{n} = 0, \quad \bar{n} \cdot n = 1. \quad (2.2)$$

Of course, we can also use other gauges since the result is gauge-invariant. However, physical picture of a DIS process is frame- and gauge-dependent. An appropriate choice of the coordinate frame and gauge is helpful to extract the evolution kernels using a simple partonic picture.

A natural derivation of the splitting function is given by TOPT in a special infinite momentum frame, i.e., the Bjorken frame, where the virtual photon has almost zero energy $q_0 = (2M\nu + Q^2)/4P$ and longitudinal momentum $q_3 = -(2M\nu - Q^2)/4P$. A Feynman

propagator is decomposed into the forward and backward propagators in TOPT, where the propagating partons stay on-shell, respectively. One can find that the contributions of the backward components of the propagators in the cut diagram, for example in Fig. 2a are suppressed [4]. Thus, the splitting function can be isolated in the equivalent particle approximation [7] as shown in Fig. 2b. To illustrate it, we parameterize the momenta in Fig. 2a as

$$p = (p_0, p_T, p_3) = (p_z, 0, p_z),$$

$$\hat{k} \simeq (zp_z + \frac{k_\perp^2}{2zp_z}, k_\perp, zp_z),$$

$$k_2 \simeq ((1-z)p_z + \frac{k_\perp^2}{2(1-z)p_z}, -k_\perp, (1-z)p_z). \quad (2.3)$$

The contributions of Fig. 2a to the twist-2 coefficient functions are

$$\begin{aligned} C_{TOPT}^{twist-2} &= \int \frac{d^3\vec{k}_2}{(2\pi)^3} \frac{1}{8E_{\hat{k}}E_{k_2}} \left[\frac{1}{E_{\hat{k}} + E_{k_2} - E_p} \right]^2 |\overline{M}(q \rightarrow qg)|^2 \\ &\times \frac{E_p}{E_{\hat{k}}} \overline{M}(\gamma^* q \rightarrow \gamma^* q) \frac{x_B}{Q^2} \delta(z - x_B), \end{aligned} \quad (2.4)$$

where we used

$$\begin{aligned} &Tr[\gamma_\mu \not{k}_1 \gamma_\nu \not{\hat{k}} \gamma_\beta \not{k}_2 \gamma_\alpha \not{\hat{k}}] \\ &= Tr[\gamma_\mu \not{k}_1 \gamma_\nu \not{\hat{k}}] Tr[\gamma_\beta \not{k}_2 \gamma_\alpha \not{\hat{k}}], \end{aligned} \quad (2.5)$$

since the momentum \hat{k} is on-shell. Now we can separately define a splitting function

$P_{TOPT}^{q \rightarrow q}$ (Fig. 2b) as

$$\begin{aligned}
& \frac{\alpha_s}{2\pi} \frac{dk_T^2}{k_T^2} P_{TOPT}^{q \rightarrow q} \\
&= \frac{1}{8E_{\hat{k}}E_{k_2}} \left[\frac{1}{E_{\hat{k}} + E_{k_2} - E_p} \right]^2 |\overline{M}(q \rightarrow q)|^2 \frac{d^3\vec{k}_2}{(2\pi)^3},
\end{aligned} \tag{2.6}$$

i.e.,

$$P_{TOPT}^{q \rightarrow q} = \frac{4}{3} \left(\frac{1+z^2}{1-z} \right). \tag{2.7}$$

The same splitting function can be obtained in a covariant framework [8]. The related dominant Fynmann diagram for the coefficient function at the $LLA(Q^2)$ is shown in Fig. 3. For convenience, we take a collinear (infinite momentum) frame, in which the momenta of the initial parton and virtual photon are parameterized as

$$p = (p_z, \vec{0}, p_z) \equiv p_+ \overline{n},$$

and

$$q \equiv q_+ \overline{n} + q_- n \equiv -x_B p_+ \overline{n} + \frac{Q^2}{2x_B p_+} n. \tag{2.8}$$

The contributions of the $q \rightarrow qg$ process in Fig. 3 to the coefficient function are

$$\begin{aligned}
& C_{CVPT}^{twist-2} \\
&= \sum_i e_i^2 \int \frac{d^4k}{(2\pi)^3} \frac{\delta((k+q)^2) \delta((p-k)^2)}{k^4} \overline{M}(\gamma^* q \rightarrow \gamma^* q),
\end{aligned} \tag{2.9}$$

where

$$\overline{M}(\gamma^* q \rightarrow \gamma^* q)$$

$$= g^2 < \frac{4}{3} >_{colour} \frac{1}{4} Tr[\gamma_\mu \gamma \cdot k_1 \gamma_\nu \gamma \cdot k \gamma_\beta \gamma \cdot p \gamma_\alpha \gamma \cdot k] \Gamma_{\alpha\beta}(k_2) d_\perp^{\mu\nu}. \quad (2.10)$$

$\Gamma_{\alpha\beta}$ is an axial gauge gluon polarization

$$\Gamma_{\mu\nu}(k) = g_{\mu\nu} - \frac{k_\mu n_\nu + k_\nu n_\mu}{k \cdot n}. \quad (2.11)$$

In the calculations we use the Sudakov variables

$$k_\mu = bp_\mu + cq'_\mu + k_{\perp\mu}, \quad (2.12)$$

where two parameters are determined by the on-shell conditions

$$b = x_B - (1 - x_B) \frac{Q^2}{2p \cdot q}, \quad (2.13)$$

and

$$c = \frac{Q^2}{2p \cdot q}. \quad (2.14)$$

The result in the leading logarithmic region, where $k^2 \ll Q^2$ are

$$C_{CVPT}^{twist-2} = \sum_i e_i^2 \frac{\alpha_s}{2\pi} \int \frac{dk_\perp^2}{k_\perp^2} \frac{4}{3} \frac{1 + x_B^2}{1 - x_B}. \quad (2.15)$$

The splitting function Eq. (2.7) can be directly obtained through dividing the coefficient function $C_{CVPT}^{twist-2}$ by the contributions of a bare photon-quark vertex (see Fig. 3b), which is

$$\begin{aligned} C_{bare}^q &= \sum e_i^2 \delta((q+p)^2) \overline{M}(\gamma^* q \rightarrow \gamma^* q) \\ &= \sum e_i^2. \end{aligned} \quad (2.16)$$

That is

$$P_{CVPT}^{q \rightarrow q} \equiv \frac{C_{CVPT}^{twist-2}}{C_{bare}^q} = \frac{4}{3} \frac{1+z^2}{1-z}, \quad (2.17)$$

in which we have taken the assumption that

$$p_+ \gg q_-, \quad (2.18)$$

thus, one can define

$$k_+ = xP_+. \quad (2.19)$$

It is not surprising of the above equivalence of two approaches. In fact, the contributions of the backward components in two off-shell Feynman propagators in Fig. 3 are suppressed under the conditions Eq. (2.18) and $LLA(Q^2)$, although straightforward computations in covariant theory do not display this fact. For confirming this conclusion, we recalculate Eq.(2.15) but removing the backward components in two Feynman propagators with the momentum k in Fig. 3. We get the same result as Eq. (2.17).

3 Twist-4 recombination functions

The recombination functions in the twist-4 evolution equations at $LL(Q^2)A$ are depicted in Fig. 1b. A simplest way of the derivation of the recombination functions is TOPT, which was developed in [4]. In this method the recombination function is isolated from the twist-4 coefficient function using the equivalent approximation as shown in Fig. 4 and it is generally written as

$$\alpha_s^2 R_{TOPT}^{(p_1 p_2 \rightarrow \hat{k})} dx_4 \frac{dk_\perp^2}{k_\perp^4} = \frac{1}{16\pi^2} \frac{x_3 x_4}{(x_1 + x_2)^3} |M_{p_1 p_2 \rightarrow \hat{k} k_2}|^2 dx_4 \frac{dk_\perp^2}{k_\perp^4}, \quad (3.1)$$

where $k_\perp^2 = k_x^2 + k_y^2$ and we use a current (the dashed lines) $-\frac{1}{4}F^{i\mu\nu}F_{\mu\nu}^i$ to probe the gluonic current [8].

The momenta of the initial and final partons are parameterized as

$$\begin{aligned} p_1 &= [x_1 p, 0, 0, x_1 p], \quad p_2 = [x_2 p, 0, 0, x_2 p], \\ \hat{k} &= [x_3 p + \frac{k_\perp^2}{2x_3 p}, k_\perp, x_3 p], \quad k_2 = [x_4 p + \frac{k_\perp^2}{2x_4 p}, -k_\perp, x_4 p], \\ k_3 &= [(x_4 - x_2)p + \frac{k_\perp^2}{2x_4 p}, -k_\perp, (x_4 - x_2)p], \\ k_4 &= [(x_4 - x_2)p + \frac{k_\perp^2}{2x_4 p}, -k_\perp, (x_4 - x_2)p]. \end{aligned} \quad (3.2)$$

For example, the recombination function for $GG \rightarrow G$ at t -channel is

$$\begin{aligned} R_{TOPT}^{GG \rightarrow G} &= \frac{g^4}{4} \langle \frac{9}{8} \rangle_{color} \frac{x_3 x_4}{(x_1 + x_2)^3} C_{\alpha\lambda\rho} C_{\beta\eta\sigma} C_{\alpha'\lambda'\rho'} C_{\beta'\eta'\sigma'} d_\perp^{\rho\rho'} d_\perp^{\sigma\sigma'} \\ &\times \frac{\Gamma_{\lambda\beta}(k_3) \Gamma_{\lambda'\beta'}(k_4)}{k_3^2 k_4^2} \left(\delta^{lm} - \frac{k_3^l k_3^m}{|\vec{k}_3|^2} \right) \left(\delta^{rs} - \frac{k_4^r k_4^s}{|\vec{k}_4|^2} \right), \end{aligned} \quad (3.3)$$

where l, m, r, s are the space indices of $\alpha, \eta, \alpha', \eta'$ of k_3 and k_4 , respectively; $C_{\alpha\lambda\rho}$ and $C_{\beta\eta\sigma}$ are triple gluon vertex. A set of recombination functions are listed in Table I.

Now we return to discuss the recombination functions in CVPT. The gluon recombination functions in the GLR-MQ evolution equation are derived using CVPT at the double leading logarithmic approximation (*DLLA*), i.e., at the small x limit [2]. We use the same way to recompute the recombination functions but in whole x region.

The coefficient function containing the gluon recombination function can be written as

$$C_{CVPT}^{GG \rightarrow G} = \int \frac{d^3 k}{(2\pi)^3} \delta(k_1^2) \delta(k_2^2) |M_{GG \rightarrow G}|^2. \quad (3.4)$$

In the t -channel,

$$|M_{GG \rightarrow G}|^2 = \frac{g^4}{4} \left\langle \frac{9}{8} \right\rangle_{color} C^{\alpha\rho\lambda} C^{\beta\eta\sigma} C^{\alpha'\rho'\lambda'} C^{\beta'\eta'\sigma'} v^{\mu\mu'} v^{\nu\nu'} d_{\perp}^{\rho\rho'} d_{\perp}^{\sigma\sigma'} \\ \frac{\Gamma_{\lambda\beta}(k_3) \Gamma_{\lambda'\beta'}(k_4) \Gamma_{\mu'\nu'}(k_1) \Gamma_{\mu\alpha}(k) \Gamma_{\nu\alpha'}(k) \Gamma_{\eta\eta'}(k_2)}{k^4 k_3^2 k_4^2}$$

where the current-gluon vertex v is

$$v^{\mu\nu} = k_{\nu} k_{1\mu} - g_{\mu\nu} k \cdot k_1, \quad (3.5)$$

and

$$\Gamma_{\lambda\beta}(k_3) = g_{\lambda\beta} - \frac{k_{3\lambda} n_{\beta} + k_{3\beta} n_{\lambda}}{k_3 \cdot n} = d_{\perp}^{\lambda\beta} - 2 \frac{k_3^-}{k_3^+} n^{\lambda} n^{\beta}. \quad (3.6)$$

The coefficient function of the contributions of a bare gluonic vertex is

$$C_{bare}^G = \frac{x_B}{2Q^2}. \quad (3.7)$$

Thus, the recombination function

$$R_{CVPT}^{GG \rightarrow G} \equiv \frac{C_{CVPT}^{GG \rightarrow G}}{C_{bare}^G}. \quad (3.8)$$

The set of recombination functions using the above mentioned CVPT method are given in Table II. A surprising result is that the recombination functions with the IR singularities in the CVPT method are inconsistent with that in the TOPT method. We shall detail it in the following section.

4 IR safety in the recombination functions

At first step, we point out that the IR singularities in R_{CVPT} originate from the gauge term in the gluon propagator $\Gamma^{\lambda\beta} = g^{\lambda\beta} - (k_3^\lambda n^\beta + k_3^\beta n^\lambda)/k_3 \cdot n$, where $k_3 \cdot n \sim y - x$ arises divergence if $y \rightarrow x$.

We decompose the propagator with the momentum k on the two gluon legs according to TOPT in Fig. 5. The on-shell propagating momenta are

$$k \rightarrow \hat{k}_F(zp_+, \bar{n}, \frac{k_\perp^2}{2zp_+}n, k_\perp), \quad (4.1)$$

and

$$\hat{k}_B(\frac{k_\perp^2}{2zp_+}\bar{n}, zp_+n, k_\perp). \quad (4.2)$$

Where the sub-indices F and B refer to the forward and backward propagations, respectively. The dominant contributions in the $LLA(Q^2)$ are from those terms with the highest power of k_\perp^2 in the numerator of the propagator. Obviously, terms n^λ or $d_\perp^{\lambda\beta}$ in Eq. (3.6) can combine with \hat{k}_B or \hat{k}_F in Eqs. (4.1) and (4.2) through the quark-gluon or triple-gluon vertex, respectively. In consequence, the contributions from the forward and backward components are coexist in the two propagators with the momentum k in these diagrams.

It is different from the recombination functions $R_{CVPT}^{GG \rightarrow G}$, the dominant numerator factor $\gamma \cdot \bar{n}$ in $R_{CVPT}^{GG \rightarrow q}$ only chooses \hat{k}_F in Eq. (4.2). Therefore, the contributions from the backward components are suppressed at the $LLA(Q^2)$ and the equivalent particle approximation is available as in $R_{TOPT}^{GG \rightarrow q}$.

Such gauge singularities also exist in the derivation of the GLR-MQ equation [2], where an unusual $i\epsilon$ prescription is used at limit $x \ll 1$ and the result is finite after taking

the principal value. Obviously, the contributions from the backward components in the gluon propagators can not be entirely excluded in this way. Thus, we can conclude that the recombination functions in the GLR-MQ equation are really a part of the twist-4 coefficient functions but not the evolution kernels for parton distribution functions(PDFs) since two legs in Fig. 5 are off-shell.

Of course, any physical results are IR safe. The IR divergences should be cancelled by summing up all related diagrams, including interference and virtual diagrams (see Fig. 6). After that one can isolate the recombination functions from the coefficient functions in the covariant framework. However, at moment there is no available covariant way to calculate the virtual and interference diagrams like Fig. 6. In the GLR-MQ equation such summations are evaluated using the Abramowsky-Gribove-Kancheli (AGK) cutting rule [9]. However, this application of the AGK cutting rule has been argued in Ref. [4]. Besides, the AGK cutting rules only change a relative weight in the contributions of the real diagrams and they can not cancel any IR divergences.

Fortunately, the TOPT approach in the Bjorken frame provides an available method to derive the recombination functions. In fact, the recombination functions can be safely separated from the twist-4 coefficient functions in this way, since the backward components in two parton legs with the momentum k are suppressed. Thus, the equivalent parton approximation can be used. Furthermore, the contributions of the gauge singular terms disappear due to the absence of these backward components. For justifying this conclusion, we use $d_{\perp}^{\mu\nu}$ to replace $\Gamma^{\mu\nu}$ in Eq. (3.3) and get the same results as Table I.

In the case that all propagators only keep their forward component in Fig. 6, the calculations of the relating interference and virtual diagrams become possible. In fact,

a simple relation among the real-, virtual- and interference diagrams is derived in Ref. [4]. Thus, we can pick up the contributions of leading recombination from all necessary cut diagrams. The resulting evolution kernel for the gluon recombination function has following form [4]:

$$\begin{aligned} & \int_{2(x_1+x_2)>x_B} dx_1 dx_2 f(x_1, x_2, Q^2) R_{TOPT}^{GG \rightarrow G}(x_1, x_2, x_B) \\ & - 2 \int_{(x_1+x_2)>x_B} dx_1 dx_2 f(x_1, x_2, Q^2) R_{TOPT}^{GG \rightarrow G}(x_1, x_2, x_B), \end{aligned} \quad (4.3)$$

where $f(x_1, x_2, Q^2)$ is the two gluon correlation function. The first and second terms in Eq. (4.3) give the antishadowing and shadowing effects in the evolutions of the parton densities.

Now let us look back to the CVPT method for the derivation of the recombination functions. According to the above mentioned discussions, we use $d_{\perp}^{\lambda\beta}$ to instead $\Gamma_{\lambda\beta}$ in Eq. (3.6). As expected, one can get the same results as Table I. From the above mentioned discussions we can conclude that the forward propagators dominate the the recombination functions.

5 Discussions and summary

An interesting question is why the IR singularities of the gluon propagator in the twist-2 coefficient function (Fig. 3a) does not break the equivalent particle approximation. We note that this propagator through the dashed line is on-shell. Thus, Eq. (2.11) can be rewritten as

$$\hat{\Gamma}^{\alpha\beta} = d_{\perp}^{\alpha\beta} - \frac{k_{\perp}^2}{k_{2+}^2} n^{\alpha} n^{\beta} \quad (5.1),$$

Now the dominant contributions to the $LL(Q^2)A$ are only from the forward components and the equivalent particle approximation is applicable.

Our discussions for the recombination functions can also be used in the investigation of the twist-4 coefficient functions [11]. One can get those functions up to dk_{\perp}^2/k_{\perp}^4 accuracy by the product of the recombination functions in Table I and the bare vertex (2.16) or (3.7).

In summary, we show that the QCD evolution kernels are frame- and gauge-independent, however, the separation of these kernels from the coefficient functions depend on the frame and gauge. The IR singularities in the recombination functions inhibit us to safely isolate the recombination functions. This result leads to the fact that the gluon recombination functions in the GLR-MQ evolution equation are unavailable. The methods avoiding the IR divergences are discussed by using the TOPT.

Acknowledgments: This work was supported by the National Natural Science Foundations of China 10075020, 90103013 and 10135060.

References

- [1] L.V. Gribov, E.M. Levin and M.G. Ryskin, Phys. Rep. 100 (1983) 1.
- [2] A.H. Mueller and J. Qiu, Nucl. Phys. B268, 427 (1986).
- [3] A. H. Mueller, Nucl. Phys. B 335, 115 (1990); A. H. Mueller, Nucl. Phys. B 415, 373 (1994).
- [4] W. Zhu, Nucl. Phys. B 551, 245 (1999) [hep-ph/9809391].
- [5] G. Sterman, G., 1993 An introduction to Quantum Field Theory, (Cambridge University Pres), 266 (1993); M.D. Scadron, Advanced Quantum theory and Its Applications Through Feynman Diagrams, eds W. Beigböck, R.P. Geroch, E.H. Lieb, T. Regge and W. Thirring (Springer-Verlag, Berlin Heidelberg), 159 (1979).
- [6] G. Altarelli and G. Parisi, Nucl. Phys. B 126, 298 (1977).
- [7] P. Kessler, Nuovo Comento 16, 809 (1966); V.N Baier, V.S. Fadin and V.A. Khoze, Nucl. Phys. 65, 381 (1973);
M.S. Chen and P. Zerwas, Phys. Rev. D12, 187 (1975).
- [8] A. Mueller, Phys. Rep. 73, 237 (1981).
- [9] V.A. Abramovsky, J.N. Gribov and O.V. Kancheli, Sov. J. Nucl. Phys. **18**, 593 (1973).
- [10] J. Blümlein, V. Ravindran, J.H. Ruan and W. Zhu, Phys. Lett. B 504, 235 (2001).

Table.1

$R_{TOPT}^{GG \rightarrow q} = R_{TOPT}^{GG \rightarrow \bar{q}}$	$\frac{1}{96} \frac{(2y-x)^2(18y^2-21yx+14x^2)}{y^5}$
$R_{TOPT}^{qq \rightarrow q}$	$\frac{2}{9} \frac{(2y-x)^2}{y^3}$
$R_{TOPT}^{q\bar{q} \rightarrow G}$	$\frac{4}{27} \frac{(2y-x)(18y^2-9yx+4x^2)}{y^3x}$
$R_{TOPT}^{GG \rightarrow G}$	$\frac{9}{64} \frac{(2y-x)(72y^4-48y^3x+140y^2x^2-116yx^3+29x^4)}{y^5x}$

Table.2

$R_{CVPT}^{GG \rightarrow q} = R_{CVPT}^{GG \rightarrow \bar{q}}$	$\frac{1}{96} \frac{(2y-x)^2(18y^2-21yx+14x^2)}{y^5}$
$R_{CVPT}^{qq \rightarrow q}$	$\frac{2}{9} \frac{(2y-x)^2(13y^2+6yx+3x^2)}{y^3(y-x)^2}$
$R_{CVPT}^{q\bar{q} \rightarrow G}$	$\frac{4}{27} \frac{(2y-x)(18y^2-9yx+4x^2)}{y^3x}$
$R_{CVPT}^{GG \rightarrow G}$	$\frac{9}{64} \frac{(2y-x)(144y^6-360y^5x+541y^4x^2-440y^3x^3+221y^2x^4-70yx^5+12x^6)}{y^5(y-x)^2x}$

Figure Captions

Fig. 1 The schematic descriptions of (a) splitting and (b) recombination functions. The solid lines are gluon or quarks and the grey ovals imply all possible QCD channels.

Fig. 2 Graphical illustration of the isolation of a splitting function in the TOPT cut diagram. \hat{k} is on-shell momentum and dashed lines refer the time order.

Fig. 3 (a) A dominate covariant Feynman diagram for the twist-2 coefficient function at the LLA ; (b) the bare virtual photon-quark vertex.

Fig. 4 Graphical illustration of the isolation of a recombination function in the TOPT cut diagram. The dashed line is an effective "current" probing the gluonic matrix.

Fig. 5 A covariant Feynman diagram containing the gluon recombination function.

Fig. 6 The virtual and interferant diagrams relating to the gluon recombination function.

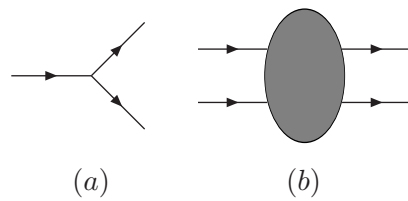


Fig.1

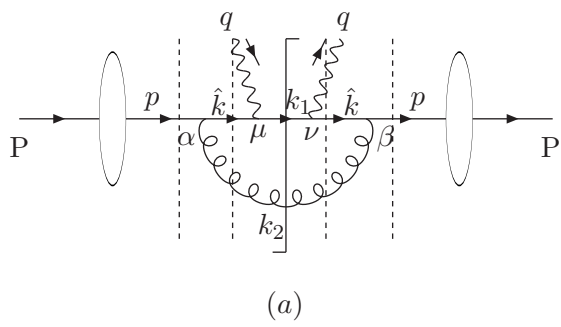
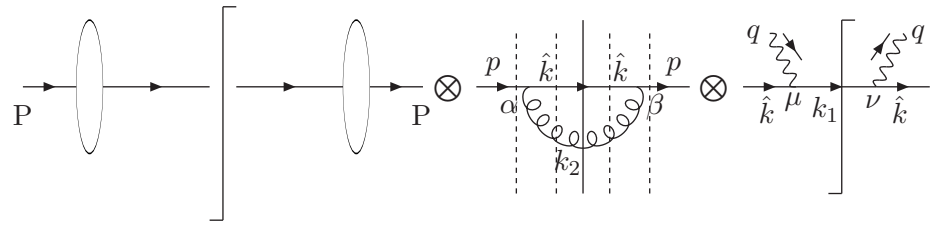


Fig.2



(b)

Fig.2

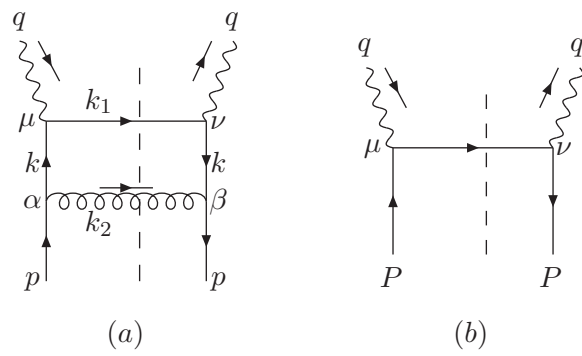


Fig.3

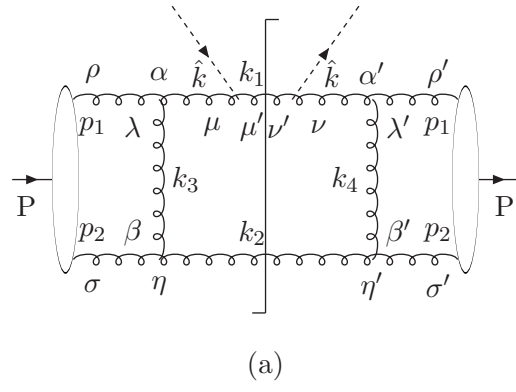
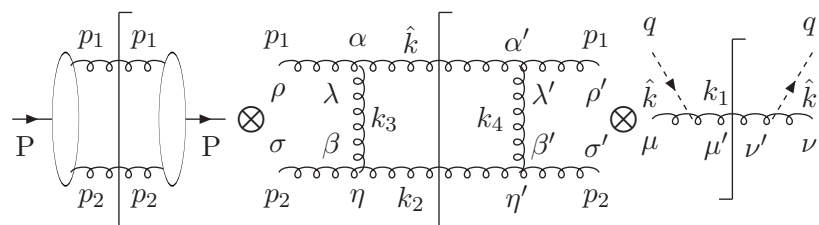


Fig.4



(b)

Fig.4



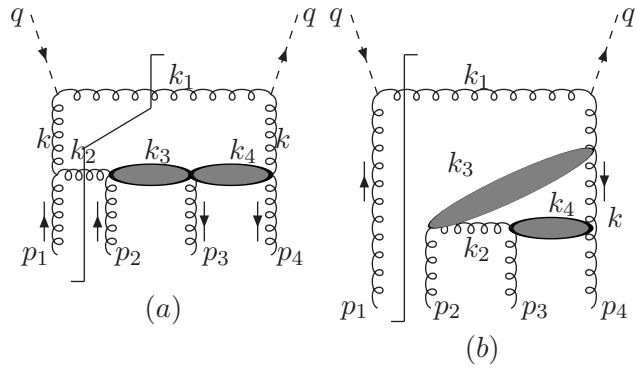


Fig.6

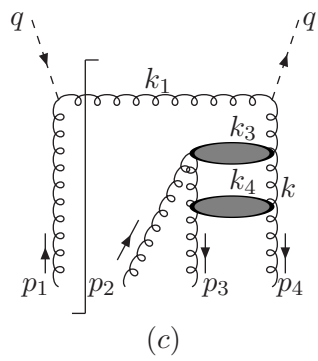


Fig.6